RESEARCH ARTICLE

QUANTUM OPTICS

Squeezing the quantum noise of a gravitational-wave detector below the standard quantum limit

Wenxuan Jia[1]*, Victoria Xu[1]*, Kevin Kuns[1], Masayuki Nakano[2], Lisa Barsotti[1], Matthew Evans[1], Nergis Mavalvala[1], members of the LIGO Scientific Collaboration†

The Heisenberg uncertainty principle dictates that the position and momentum of an object cannot be simultaneously measured with arbitrary precision, giving rise to an apparent limitation known as the standard quantum limit (SQL). Gravitational-wave detectors use photons to continuously measure the positions of freely falling mirrors and so are affected by the SQL. We investigated the performance of the Laser Interferometer Gravitational-Wave Observatory (LIGO) after the experimental realization of frequency-dependent squeezing designed to surpass the SQL. For the LIGO Livingston detector, we found that the upgrade reduces quantum noise below the SQL by a maximum of three decibels between 35 and 75 hertz while achieving a broadband sensitivity improvement, increasing the overall detector sensitivity during astrophysical observations.

A consequence of quantum mechanics is the Heisenberg uncertainty principle, which states that the product of the measurement noises of conjugate observables (such as position and momentum) cannot be less than $\hbar/2$, where $\hbar$ is the reduced Planck constant. Measuring the position x of an object with uncertainty Δx inevitably perturbs its momentum by $\Delta p \geq \hbar/(\Delta x)$. After a time τ, the object with mass m freely evolves, acquiring additional position uncertainty $\Delta x'$ from the momentum perturbation $\Delta x' = \tau\Delta p/m = \hbar\tau/(2m\Delta x)$. An extremely precise measurement ($\Delta x \to 0$) will make the next position measurement totally unpredictable ($\Delta x' \to \infty$) because of this phenomenon, which is known as quantum back action (*1*). The minimal repeatable uncertainty is achieved when $\Delta x = \Delta x' = \sqrt{\hbar\tau/(2m)}$, which is known as the standard quantum limit (SQL) (*2*, *3*). The SQL applies to measurements of microscopic particles; it is also a limiting factor for the measurements made by interferometric gravitational-wave detectors, which measure attometer-scale displacements of macroscopic mirrors (*4*).

In principle, the SQL could be surpassed by introducing quantum correlations between the interferometer's laser light and the mirrors (*5*–*7*). Proposed designs that do this are known as quantum nondemolition interferometers (*8*, *9*). One approach proposed a squeezed-input interferometer, which would surpass the SQL at a particular frequency by injecting a nonclassical state of light, known as a squeezed vacuum state, into the interferometer. The addition of a detuned Fabry-Pérot filter cavity would impose a frequency-dependent phase shift on the squeezed vacuum states reflected from it, allowing the SQL to be surpassed over a broader frequency range (*9*).

In a proof-of-principle demonstration, previous work injected squeezed vacuum states into the Laser Interferometer Gravitational-Wave Observatory (LIGO), producing quantum correlations and surpassing the SQL in a narrow frequency region (30 to 50 Hz) (*10*). However, because that experiment did not include a filter cavity, the quantum noise increased at all other frequencies, causing an overall decrease of the astrophysical sensitivity (*10*), as theoretically predicted (*9*). Subsequently, a 300-m-long filter cavity was added to both LIGO Livingston (L1) and Hanford (H1) interferometers, which was designed to extend the reduction of quantum noise over a broader frequency range (*11*). We examined the quantum noise performance of the LIGO L1 interferometer operating with this filter cavity.

Simplified quantum noise model

Gravitational-wave modulations of spacetime are quantified by the dimensionless strain h. A gravitational-wave detector converts these modulations into a measurable differential displacement between two pairs of suspended mirrors. In this case, Δx is the interferometer differential displacement, and $h = \Delta x/L_{\mathrm{arm}}$, where L_{arm} is the length of each interferometer arm (4 km for LIGO). At measurement frequencies, the interferometer mirrors move freely, so the SQL for these mirrors can be expressed by considering the gravitational-wave strain noise amplitude spectral density

$$h_{\mathrm{SQL}}(\Omega) = \frac{\Delta x_{\mathrm{SQL}}(\Omega)}{L_{\mathrm{arm}}} = \sqrt{\frac{2\hbar}{(m/4)\Omega^2}}\frac{1}{L_{\mathrm{arm}}} \quad (1)$$

where Ω is the measurement frequency. This strain limit depends on the mass of the object rather than the number of photons used to probe its position (determined by the laser power). In LIGO, the effective mass of the object is the reduced mass ($m/4$) of the differential motion of each pair of arm cavity mirrors, each 40 kg, so

$$h_{\mathrm{SQL}}(\Omega) \approx 1.8 \times 10^{-24}\left(\frac{2\pi \times 100\ \mathrm{Hz}}{\Omega}\right)\frac{1}{\sqrt{\mathrm{Hz}}} \quad (2)$$

For clarity, we first present a simplified model of quantum noise in the LIGO interferometers developed in previous work (*11*). In the ideal lossless case, the power spectral density (PSD) of quantum noise $S(\Omega)$ can be expressed as

$$S(\Omega) = \frac{h_{\mathrm{SQL}}^2(\Omega)}{2}\left[\mathcal{K}(\Omega) + \frac{1}{\mathcal{K}(\Omega)}\right] \quad (3)$$

where $\mathcal{K}(\Omega)$ is the opto-mechanical coupling strength; the first term represents noise from quantum back action, and the second term represents imprecision from photon shot noise. $\mathcal{K}(\Omega)$ increases with the circulating laser power in arm cavities P_{arm} as

$$\mathcal{K}(\Omega) = \frac{16k_0P_{\mathrm{arm}}}{m\gamma_0L_{\mathrm{arm}}}\frac{1}{\Omega^2}\left(1 + \frac{\Omega^2}{\gamma_0^2}\right)^{-1} \quad (4)$$

where $k_0 = 2\pi/(1064\ \mathrm{nm})$ is the laser wave number, and $\gamma_0 \approx 2\pi \times 450$ Hz is the detector's signal bandwidth.

At frequencies below 40 Hz, measurement back action dominates because of the strong opto-mechanical coupling [$\mathcal{K}(\Omega) \gg 1$]. At frequencies above γ_0, the opto-mechanical coupling is weak [$\mathcal{K}(\Omega) \ll 1$], so the measurement imprecision noise dominates. The frequency at which these two forms of quantum noise contribute equally to the total quantum noise is called the SQL frequency Ω_{SQL}, defined as $\mathcal{K}(\Omega_{\mathrm{SQL}}) = 1$. The value of Ω_{SQL} scales with the square root of the laser power; for a circulating power of $P_{\mathrm{arm}} = 260$ kW, $\Omega_{\mathrm{SQL}} = 2\pi \times 37$ Hz.

Together, these two forms of quantum noise enforce the SQL for displacement sensing (Eq. 3), which arises from the use of uncorrelated photons to probe mirror positions. Equation 3 enforces the SQL because it is an incoherent superposition of quantum back action and imprecision noise. In the presence of quantum correlations between light and mirrors, Eq. 3 no longer holds, allowing the SQL to be surpassed.

Squeezed vacuum is a nonclassical state of light that uses quantum correlations between photon pairs to reduce one form of quantum

[1]Laser Interferometer Gravitational-Wave Observatory (LIGO) Laboratory, Massachusetts Institute of Technology, Cambridge, MA 02139, USA. [2]LIGO Livingston Observatory, Livingston, LA 70754, USA.
*Corresponding author. Email: wenxuanj@mit.edu (W.J.); victoriaa.xu@ligo.org (V.X.)
†LIGO Scientific Collaboration authors and affiliations are listed in the supplementary materials.

noise at the expense of the other, in a way allowed by the Heisenberg uncertainty principle (*12*). During LIGO's third observing run, frequency-independent squeezing was injected into the interferometer to reduce the imprecision noise while increasing the quantum back action noise (*13*). The injection of squeezed vacuum (denoted by subscript SQZ) into the output port of an interferometer (*14*) modified its quantum noise relative to Eq. 3, to produce

$$S_{\mathrm{SQZ}}(\Omega) = S(\Omega)\{e^{-2r}\cos^2[\phi - \theta(\Omega)] + e^{2r}\sin^2[\phi - \theta(\Omega)]\} \quad (5)$$

where e^{-2r} is the squeezing factor, the amount by which the injected quantum noise is squeezed relative to vacuum noise; ϕ is the relative phase between the input squeezed field and the interferometer field (known as the squeeze angle); and $\theta(\Omega) = \tan^{-1}\mathcal{K}(\Omega)$ is the squeeze angle rotation due to the opto-mechanical response of the interferometer.

Frequency-dependent squeezed states (denoted by subscript FDSQZ) vary the input squeeze angle as a function of frequency $\phi \rightarrow \phi(\Omega)$. They can be prepared by reflecting the frequency-independent squeezed state from a detuned and overcoupled Fabry-Pérot cavity (*11*, *15*–*17*). When the filter cavity linewidth is matched to Ω_{SQL}, it imparts a phase rotation $\phi(\Omega) \approx \theta(\Omega) = \tan^{-1}\mathcal{K}(\Omega)$ on the reflected squeezed vacuum states, which enables quantum noise reduction of e^{-2r} at all frequencies (*18*)

$$S_{\mathrm{FDSQZ}}(\Omega) = \frac{h^2_{\mathrm{SQL}}(\Omega)}{2}\left[\mathcal{K}(\Omega) + \frac{1}{\mathcal{K}(\Omega)}\right]e^{-2r} \quad (6)$$

At the frequency Ω_{SQL}, this approach is predicted to reduce quantum noise below the SQL by a factor of e^{-2r}

$$S_{\mathrm{FDSQZ}}(\Omega_{\mathrm{SQL}}) = h^2_{\mathrm{SQL}}(\Omega_{\mathrm{SQL}})e^{-2r} \quad (7)$$

Experimental setup

We provide in Fig. 1 a simplified diagram of the LIGO interferometer (*19*) during the fourth astrophysical observing run (O4), which began in 2023. It includes Fabry-Pérot arm cavities formed by a pair of 40-kg mirrors to resonantly enhance strain sensitivity, input power recycling to increase the circulating laser power [and thus $\mathcal{K}(\Omega)$], and output signal extraction to broaden the detection bandwidth. Components of the squeezing system, comprising the squeezed vacuum source (squeezer) and the filter cavity, are also shown.

Squeezed vacuum was injected at the output port of the interferometer to reduce quantum noise (*20*). The LIGO squeezer generates frequency-independent squeezed vacuum states through spontaneous parametric down-conversion of 532-nm photons in a bow-tie optical parametric amplifier cavity containing a nonlinear crystal (*13*, *21*). The 300-m filter cavity was controlled so that its resonance frequency is detuned with respect to the carrier frequency of the main laser, thus producing frequency-dependent squeezing [$\phi \rightarrow \phi(\Omega)$] before injection into the interferometer (*11*). A movable beam diverter was placed in the squeezed vacuum beam path before injection into the interferometer. Squeezing could be injected or blocked by opening or closing the beam diverter.

Measuring quantum noise below the SQL

Our inferred quantum noise of the L1 detector operating with frequency-dependent squeezing is shown in Fig. 2. We found that the quantum noise surpasses the SQL between 35 and 75 Hz, by a maximum of 3 dB near 50 Hz. Determining the squeezed quantum noise below 100 Hz is complicated by the presence of non-quantum (classical) noise that is a factor of two times greater in amplitude (*19*). We performed a two-step analysis to infer the squeezed quantum noise from measurements of the total noise.

First, we inferred the classical noise by subtracting an unsqueezed quantum noise model from measurements of the total detector noise with squeezing disabled. The unsqueezed quantum noise model has several degenerate parameters. For example, the circulating laser power in the arm cavity and optical loss in the readout path have the same phenomenological effect on the imprecision noise. To constrain the parameter space, we experimentally set 11 constant squeezing angles ϕ, because the quantum noise S_{SQZ} depends strongly on ϕ (Eq. 5), then found a single set of interferometer parameters that simultaneously matches the measured noise for every value of ϕ. We performed Markov Chain Monte Carlo inference (*22*) to determine the best-fitting set of parameters that match all 11 different squeeze angle datasets. Sensitivity measurements for the three values of ϕ that dip below the SQL are shown in Fig. 3 (data for all 11 ϕ values are shown in fig. S2). Compared with the simplified model presented above, this numerical noise model used for subtraction includes experimental degradations such as squeezing phase noise, optical loss, and mode-mismatch across the various cavities of the interferometer (*23*–*25*).

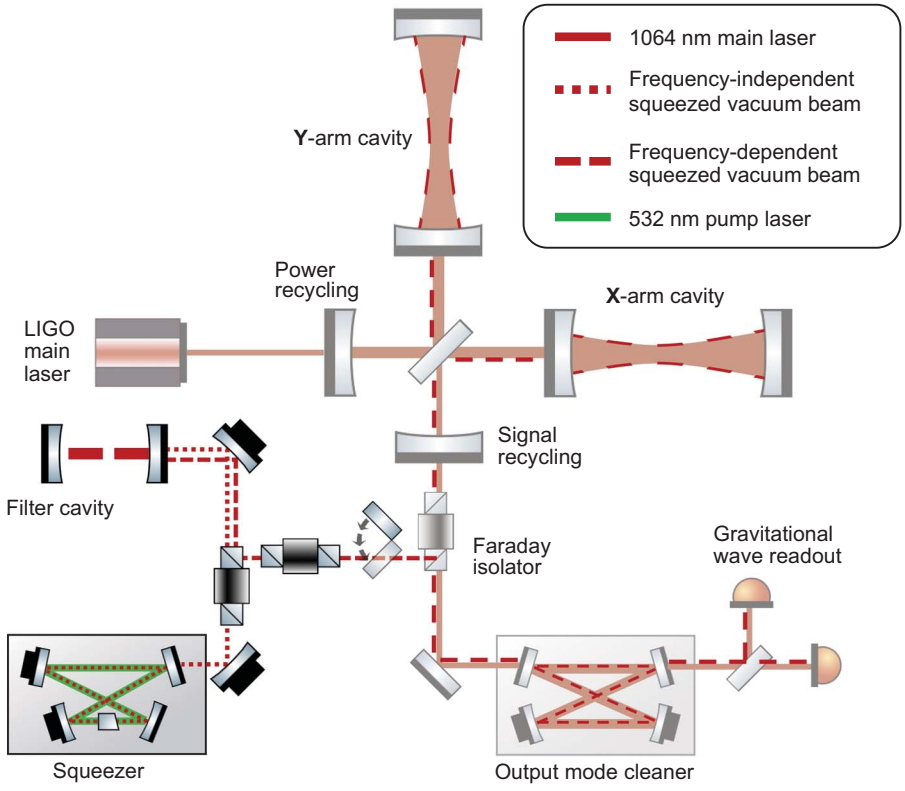

Fig. 1. Simplified schematic of the LIGO interferometer. The filter cavity was installed for the fourth astrophysical observing run (O4), which began in 2023. The squeezing system (saturated color) is shown overlaying the main interferometer (shaded color), which has 4-km-long arm cavities. Except the main laser, all optical components are suspended in ultrahigh vacuum. Frequency-independent squeezed vacuum (dotted red line) is generated by an optical parametric amplifier (labeled squeezer), which consists of a nonlinear optical crystal in a dually resonant bow-tie cavity. The outgoing squeezed beam is reflected from a 300-m-long filter cavity to produce frequency-dependent squeezing (dashed red line), injected with a Faraday isolator through a beam diverter that can be opened or closed (gray arrows), then propagated through the full LIGO interferometer before detection at the two readout photodiodes.

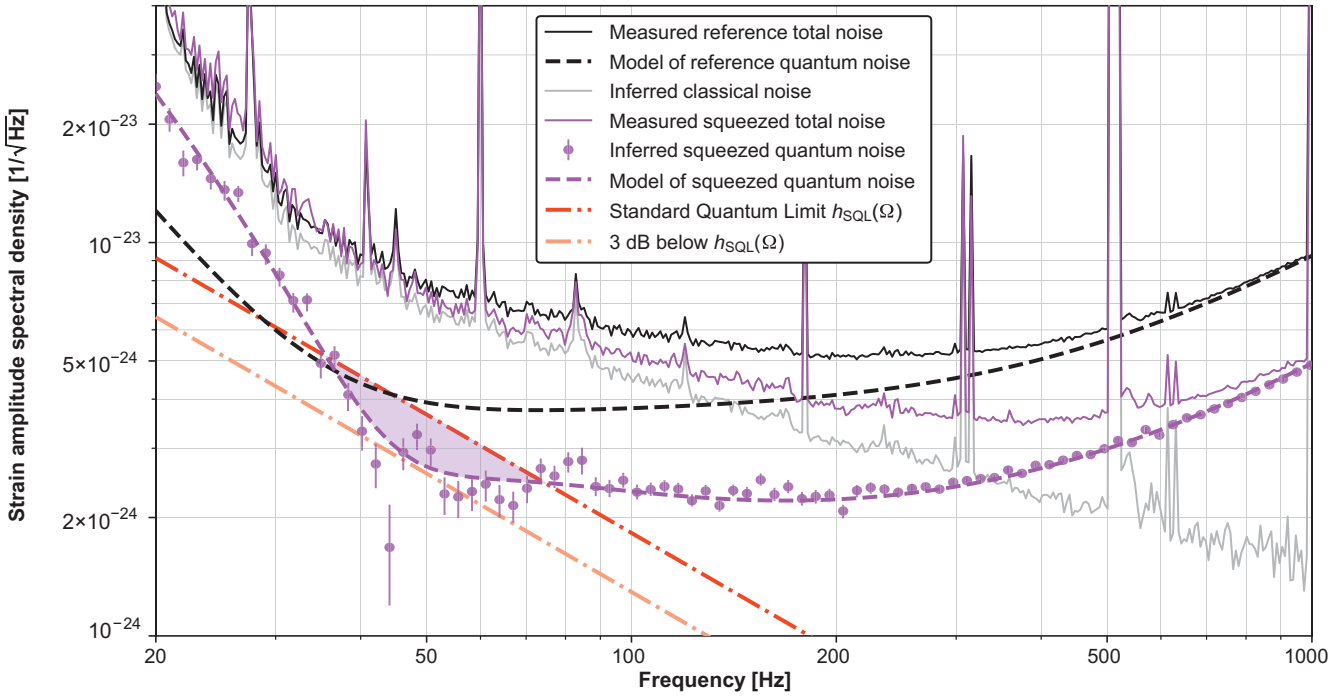

Fig. 2. Measured sensitivity of the LIGO L1 interferometer. Data were measured with a detector configuration representative of the nominal detector noise during O4. The total detector noise spectrum is an incoherent sum of the classical and quantum noise. The unsqueezed reference total noise (solid black line) was measured without squeezing injection. An unsqueezed quantum noise model (dashed black line) was subtracted from the measured reference total noise to estimate the underlying classical noise (gray line). The classical noise estimate was then subtracted from the measured squeezed total noise spectra (solid purple line) to infer the squeezed quantum noise (purple dots, with error bars indicating 1σ uncertainty). A model of the frequency-dependent squeezed quantum noise (purple dashed line) was fitted to the data points by adopting the same detector parameters and allowing squeezer parameters to vary. The red dot-dashed line indicates the theoretical SQL, and the orange dot-dashed line is 3 dB below it. We found that the squeezed quantum noise surpasses the SQL between 35 and 75 Hz (purple-shaded region), by a maximum of 3 dB.

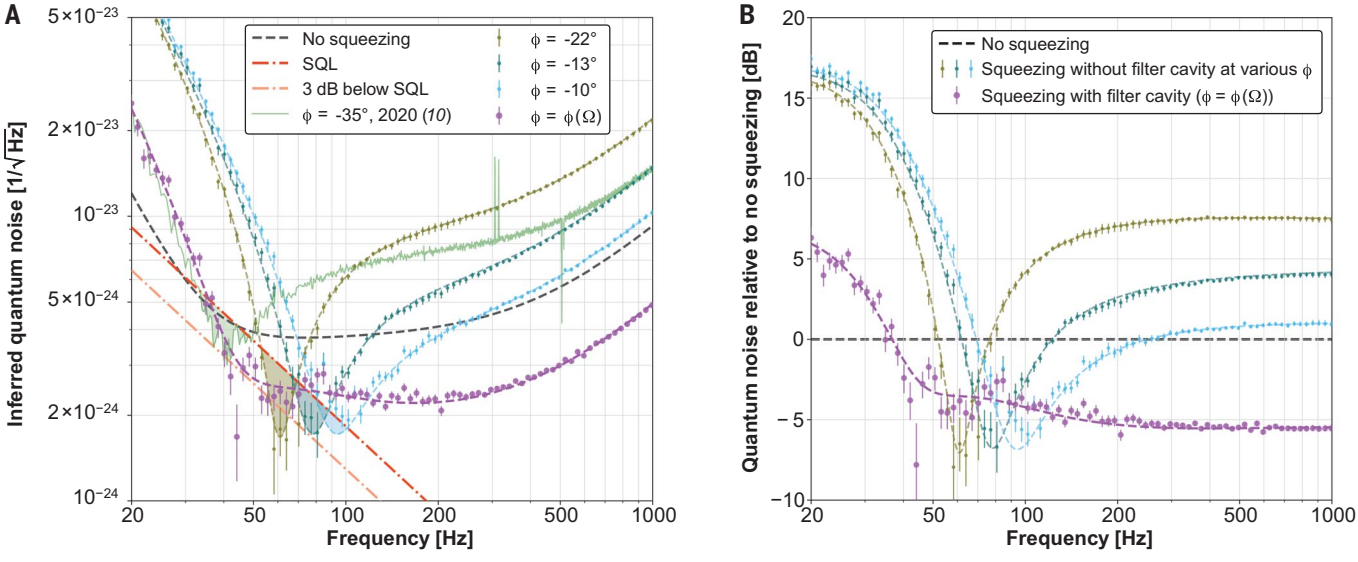

Fig. 3. Quantum noise reduction with and without the filter cavity. (**A** and **B**) Quantum noise reduction expressed as (A) strain noise and (B) decibels relative to the unsqueezed quantum noise model (dashed black line, as in Fig. 2). In (A) and (B), data points show the quantum noise inferred from total detector noise measurements; error bars indicate the 1σ uncertainty. Dashed lines indicate quantum noise models fitted to the data. The input filter cavity rotates the injected squeezing angle ϕ as a function of frequency to produce frequency-dependent squeezing, ϕ → ϕ(Ω) (*9*). Frequency-independent squeezing spectra (olive, teal, and blue) were measured for three injected squeeze angles ϕ, with the filter cavity end mirror misaligned. These spectra outline the minimum quantum noise achievable with injected squeezing. The green line in (A) was measured before filter cavity installation (*10*). The purple line indicates the quantum noise with frequency-dependent squeezing. The installed filter cavity (*11*) delivers broadband quantum noise reduction, including where quantum noise surpasses the SQL [red dot-dashed line in (A)].

Second, we subtracted the classical noise estimate from subsequent measurements of the total detector noise with squeezing enabled to infer the squeezed quantum noise, which is our measurement of $\sqrt{S_{SQZ}(\Omega)}$ from Eq. 5. The two-step noise subtraction process assumes that classical noise remains identical between the unsqueezed and squeezed modes of operation. Any variations in classical noise between these modes are incorporated as estimation uncertainties. We used previously determined uncertainty propagation methods (*10*) to estimate the total uncertainty budget, including statistical uncertainties from detector noise PSD estimation and nonstationary classical noise, and the systematic uncertainties from calibration and residual model errors (*22*).

Statistical uncertainties from PSD estimation and nonstationary classical noise (*26*) limited estimates of low-frequency quantum noise. We interleaved multiple 20-min segments of unsqueezed and squeezed measurements to control for time variations of the classical noise. The total detector noise measured with 1 hour of combined data segments in the unsqueezed and squeezed configurations is shown in Fig. 2. We found that the difference in the classical noise between segments (uncertainty from nonstationarity) is commensurate with the total uncertainty from 1 hour of PSD estimation with optimal frequency binning (fig. S4).

We performed a full derivation of the total uncertainty budget (*22*). The main systematic uncertainty arises from the real-time calibration process, which applies a known force to the mirror to actively modulate the strain and measure the instrument's response (*27*, *28*). For the data used in our measurements, the systematic uncertainties are less than 5% (fig. S4).

Squeezing with and without the filter cavity

We show in Fig. 3 L1 measurements of the inferred quantum noise with frequency-dependent squeezing and frequency-independent squeezing at three injected squeeze angles ϕ. The data are presented as strain noise (Fig. 3A) and as decibels of quantum noise reduction (Fig. 3B) compared with no squeezing (the decibel noise reduction is defined as $20\log_{10}\left[\sqrt{S_{SQZ}(\Omega)}/S(\Omega)\right]$). We also show in Fig. 3 numerical quantum noise models that use the best-fitting experimental parameters for the full interferometer and squeezer. The close agreement between the model curves and measured spectra supports the unsqueezed quantum noise model used for subtraction. We then extended the model to include the filter cavity parameters (*11*). The quantum noise model for frequency-dependent squeezing is consistent with the inferred quantum noise spectra.

Compared with frequency-independent squeezing, an ideal filter cavity would rotate the injected squeezing angle as a function of frequency, $\phi \rightarrow \phi(\Omega) \approx \tan^{-1}\mathcal{K}(\Omega)$, to reduce the quantum noise by a factor of e^{-2r} at all frequencies, as in Eq. 6. That would provide a single configuration that reaches the envelope of sub-SQL quantum noises achievable by all frequency-independent squeezing spectra. However, there is a discrepancy between the noise reduction achieved with frequency-independent squeezing and with the frequency-dependent squeezing provided by the filter cavity, especially between 20 and 200 Hz (Fig. 3). The inclusion of the filter cavity reduces the quantum noise across a broader range of frequencies than squeezed light alone (Fig. 3B) but not by as much as the theoretically predicted e^{-2r} reduction of quantum noise at all frequencies.

We ascribe this nonoptimal performance to a mismatch between the SQL frequency and the filter cavity linewidth. Assuming a lossless cavity, an optimal filter cavity would have its half-width-at-half-maximum linewidth γ_{FC} and detuning δ_{FC} both matched to the SQL frequency, so that $\gamma_{FC} = \delta_{FC} = \Omega_{SQL}/\sqrt{2}$ (*18*). The installed filter cavity was designed to have $\gamma_{FC} = 2\pi \times 42$ Hz, by using an input coupler power transmissivity $T_{in} \approx 1000$ parts per million (ppm) (*11*) and assuming 60 ppm optical loss, to approximately match $\Omega_{SQL} = \sqrt{2}\gamma_{FC} = 2\pi \times 59$ Hz. However, our measurements indicate that the SQL frequency is $\Omega_{SQL} = 2\pi \times 37$ Hz, which is a factor of 1.6 less than that of the design.

We conclude that with frequency-dependent squeezing, the LIGO detectors operated with quantum-limited sensitivity that surpasses the SQL during astrophysical observing. With the squeezing rotation imparted by the current filter cavity, we show that squeezing directly increases detector sensitivity by 5.6 dB at kilohertz frequencies while yielding strain sensitivities that surpass the SQL around 50 Hz. This experimentally demonstrates a theoretically proposed improvement to gravitational-wave detectors (*9*). Our analysis was sufficient to model the quantum noise through the complex optical systems of the LIGO interferometer, which matches the experimental data across a wide range of input squeeze angles. The injection of quantum squeezing allowed us to probe the detector configuration and expand the astrophysical reach of gravitational-wave observations.

REFERENCES AND NOTES

1. V. B. Braginsky, Y. I. Vorontsov, K. S. Thorne, *Science* **209**, 547–557 (1980).
2. V. B. Braginski, *Sov. Phys. J. Exp. Theor. Phys.* **26**, 831 (1968).
3. V. B. Braginsky, F. Y. Khalili, K. S. Thorne, *Quantum Measurement* (Cambridge Univ. Press, 1992).
4. The LIGO Scientific Collaboration *et al*., *Class. Quantum Gravity* **32**, 074001 (2015).
5. W. G. Unruh, in *Quantum Optics, Experimental Gravity, and Measurement Theory*, P. Meystre, M. O. Scully, Eds., NATO Advanced Science Institutes Series (Springer, 1983), pp. 647–660.
6. W. G. Unruh, in *Quantum Optics, Experimental Gravity, and Measurement Theory*, P. Meystre, M. O. Scully, Eds., NATO Advanced Science Institutes Series (Springer, 1983), pp. 637–645.
7. H. P. Yuen, *Phys. Rev. Lett.* **51**, 719–722 (1983).
8. Quantum nondemolition measurements are those with quantum noise below the SQL (*9*). In some circumstances, this definition differs from that used in other fields of physics, in which a quantum nondemolition measurement implies a measurement with no quantum back action on the measured observable (*1*, *3*, *29*, *30*).
9. H. J. Kimble, Y. Levin, A. B. Matsko, K. S. Thorne, S. P. Vyatchanin, *Phys. Rev. D* **65**, 022002 (2001).
10. H. Yu *et al*., *Nature* **583**, 43–47 (2020).
11. D. Ganapathy *et al*., *Phys. Rev. X* **13**, 041021 (2023).
12. R. Schnabel, *Phys. Rep.* **684**, 1–51 (2017).
13. M. Tse *et al*., *Phys. Rev. Lett.* **123**, 231107 (2019).
14. C. M. Caves, *Phys. Rev. D* **23**, 1693–1708 (1981).
15. L. McCuller *et al*., *Phys. Rev. Lett.* **124**, 171102 (2020).
16. Y. Zhao *et al*., *Phys. Rev. Lett.* **124**, 171101 (2020).
17. F. Acernese *et al*., Virgo Collaboration, *Phys. Rev. Lett.* **131**, 041403 (2023).
18. C. Whittle *et al*., *Phys. Rev. D* **102**, 102002 (2020).
19. A. Buikema *et al*., *Phys. Rev. D* **102**, 062003 (2020).
20. L. Barsotti, J. Harms, R. Schnabel, *Rep. Prog. Phys.* **82**, 016905 (2019).
21. S. S. Y. Chua *et al*., *Opt. Lett.* **36**, 4680–4682 (2011).
22. Materials and methods are available as supplementary materials.
23. A. Buonanno, Y. Chen, *Phys. Rev. D* **64**, 042006 (2001).
24. P. Kwee, J. Miller, T. Isogai, L. Barsotti, M. Evans, *Phys. Rev. D* **90**, 062006 (2014).
25. L. McCuller *et al*., *Phys. Rev. D* **104**, 062006 (2021).
26. D. Davis *et al*., *Class. Quantum Gravity* **38**, 135014 (2021).
27. L. Sun *et al*., *Class. Quantum Gravity* **37**, 225008 (2020).
28. S. Karki *et al*., *Rev. Sci. Instrum.* **87**, 114503 (2016).
29. V. B. Braginsky, F. Ya. Khalili, *Rev. Mod. Phys.* **68**, 1–11 (1996).
30. A. A. Clerk, M. H. Devoret, S. M. Girvin, F. Marquardt, R. J. Schoelkopf, *Rev. Mod. Phys.* **82**, 1155–1208 (2010).
31. W. Jia *et al*., Data for LIGO operates with quantum noise below the standard quantum limit. Zenodo (2024); https://pypi.org/project/gwinc.

ACKNOWLEDGMENTS

We thank V. Sudhir, D. Wilken, and H. Pfeiffer for helpful discussions. **Funding:** We acknowledge the support of the US National Science Foundation (NSF) for the construction and operation of the LIGO Laboratory and Advanced LIGO as well as the Science and Technology Facilities Council (STFC) of the United Kingdom, and the Max-Planck-Society (MPS) for support of the construction of Advanced LIGO. Additional support for Advanced LIGO was provided by the Australian Research Council. W.J. and V.X. acknowledge the LIGO Scientific Collaboration Fellows program for additional support. LIGO was constructed by the California Institute of Technology and Massachusetts Institute of Technology with funding from NSF and operates under cooperative agreement PHY-2309200. Advanced LIGO was built under award PHY-18680823459. The A+ upgrade to Advanced LIGO is supported by US NSF award PHY-1834382 and UK STFC award ST/S00246/1, with additional support from the Australian Research Council. **Author contributions:** L.B., M.E., and N.M. conceived and supervised the project. W.J. and M.N. optimized and configured the LIGO Livingston detector to collect the data. W.J., V.X., and K.K. analyzed the data, with the model developed by L.M. and K.K.; W.J., V.X., L.B., and M.E. prepared the manuscript. P. Fritschel is the chief scientist of the LIGO detector. All authors contributed to the research and development, data curation, installation, commissioning, operation, and maintenance of the LIGO detectors for observing run 4. **Competing interests:** There are no competing interests to declare. **Data and materials availability:** All numerical data shown in the figures and our MCMC analysis code are archived at Zenodo (*31*). Our best-fitting detector and squeezer model parameters are listed in table S1.

SUPPLEMENTARY MATERIALS

science.org/doi/10.1126/science.ado8069
Members of the LIGO Scientific Collaboration Authors and Affiliations
Materials and Methods
Supplementary Text
Figs. S1 to S4
Table S1
Reference (*32*)

Submitted 22 April 2024; accepted 22 July 2024
10.1126/science.ado8069